ISSN:2321-1156
International Journal of Innovative Research in Technology & Science(IJIRTS)

Numerical Simulation of Wind tunnel Blockage and Wall Interference Effects at Supersonic Mach Number Flows

A.P. Roychowdhury and C. Unnikrishnan
Aerodynamics R& D Division,
Vikram Sarabhai Space Centre,
Thiruvanthapuram, Pin 695022, Kerala , India.

Abstract

Numerical simulation of wind tunnel blockage and wall interference effects at supersonic Mach numbers on a payload fairing of a launch vehicle configuration has been studied. Axi-symmetric simulations have been done for Mach numbers of 1.5 and 3.0 for different blockage ratios using a compressible finite volume based Reynolds-averaged Navier-Stokes solver. The effect of blockage ratio on the pressure distribution on the body is shown. When the blockage ratio is small the detached shock in front of the body extends to the tunnel wall and reflects back and forth from the body and tunnel wall giving oscillations on the pressure distribution. The Mach number and pressure palettes presented clearly show the detached shock in front of the body and reflection of the shock from the tunnel wall to the body and back to the wall again. The study also brings forth information regarding the length of the body and the blockage ratio to get a smooth pressure distribution unaffected by the wind tunnel wall presence

Nomenclature

c	Speed of sound
C_p	Wall pressure Coefficient as $(p-p_\infty)/0.5\rho_\infty U_\infty^2$
d	Distance or reference length
e	Total energy per unit volume
H	Source terms
F,G	Flux vectors in the x- and r-directions
M	Mach number
P	Pressure
Pr	Prandtl number
Re	Reynolds number
q	Matrix q of terms for which N-S are being solved or heat flux
t	Time
T	Temperature or Transformation matrix
u,v	Velocity in x- and r- direction
U	Vector of conserved variables
x,r	Axial and radial coordinates
γ	Specific heat ratio
ρ	Density
μ	Coefficient of viscosity
τ	Shear stress term

Subscripts :

x,r	Axial and radial components
∞	free stream quantities
w	wall quantity

Introduction

Wind tunnel is a device for producing an air stream in a controlled conditions past models like aircraft, launch vehicles etc. in order to investigate flow on the full scale objects before the actual application. Wind tunnel testing is the backbone of the aerospace engineering field. It is a mandatory practice in aerospace industry to test the scaled model in a wind tunnel and obtain information of aerodynamic flow features and flow parameters like pressures and heat transfers on the body and extrapolate these values to the flight conditions using some dimensionality similarities like Reynolds number and Mach number equivalent principles. This information will help in the structural and thermal design of the vehicle.

High speed wind-tunnels include compressibility effects of the flow and measured in terms of Mach number rather than velocity, which is the ratio of a given velocity to that of speed of sound of flow around the body. As the speed of the flow is increased the power required are high in high speed wind tunnels and which are often the intermittent type in which energy is stored in terms of pressure or vacuum or both. These are allowed to drive the tunnel for a few seconds out of each hour of pumping. Intermittent blow-down or in-draft tunnel are used for Mach numbers 0.5 to 5.0 and intermittent pressure -vacuum tunnels are used for higher Mach number flows. Transonic flow imbed local subsonic

flow in a supersonic flow. Even today the transonic flow complexity makes it impossible to establish theories with which aerodynamic characteristics of aircraft or components can be readily predicted. Hence transonic flow wind-tunnel testing is essential to provide aerodynamic information to designers. Size is one of the limiting factor of wind-tunnels is that of power requirement hence test section is kept small and hence only scaled models of bodies are kept for testing. Wall interference effects due to shock reflection from wind tunnels need the length of test section to be small so that reflected shocks go outside the test section length and do not interfere with the flow in the test section**.** In wind tunnel testing of sub-scaled models for subsonic, transonic and supersonic flows there are two types of blockage effects viz. body blockage effects] and wall interference caused blockage effects. Results obtained from wind tunnel testing needs to be corrected for blockage effects, buoyancy, wall interference and STI (Strut, Tare and Interference) effects. The body blockage effects include Solid blockage due to model inserted in wind tunnel and Wake blockage due to higher velocity as boundary layer grows around model putting model in pressure gradient and results need to be corrected. The wall interference effects are dependent on Reynolds number and caused due to shock/boundary layer interaction

One of the major constraints in the wind tunnel testing is the size of the model to be tested as wind tunnels are small in size compared to the vehicles in question to be investigated. The size restriction includes all the dimensions of length, breadth and height. Normally the breadth and height dimension will give rise to the blockage effect in the wind tunnel testing and the length dimension will give rise to the tunnel wall interference effect. In launch vehicles the length dimensions are very large compared to the breadth and height dimensions and the wall interference effect will limit the length of the models to be tested.

In supersonic flow over typical launch vehicles with a spherical cap at the nose, the detached shock at the nose will extend to the tunnel wall. These shock waves on hitting the tunnel wall will reflect back toward the model which can again reflect back to the tunnel wall and back to the model again and multiple shock reflection phenomena can be observed if the models lengths are very large. These shocks hitting on the model can severely change the aerodynamic loads on the model from those that would be expected in free flight. Hence it is important to find out the optimum length dimension of the launch vehicle model to be tested to get accurate results without this tunnel wall interference effects. It is very difficult to know the size of the model to overcome the above mentioned tunnel wall interference effects prior to experiments though some estimates can be predicted with previous experimental studies.

With the development of modern numerical techniques along with the advent of high speed computers, Computational Fluid Dynamics popularly known as CFD has matured to a stage where complex fluid flow problems can be accurately solved in a relatively small amount of computational time. And now a day, the CFD is complementing the experimental methods in a big way and the concept of numerical wind tunnel is in the fashion. One such problem that CFD can handle and help the experimental method is the study of tunnel wall blockage and interference effect itself [1-7].

Maciejewski et al. [1] has reported the numerical simulation of the blockage effects in wind tunnel on automobile bodies using an incompressible Navier-Stokes solver and the effect of blockage on drag force is presented for different tunnel heights. Griffith et al [2] gives computational 2-D results for semi-circular blockages for laminar flows with Reynolds number 50 to 3000 for small to large blockage ratio cases for very low speed which can be used for better understanding of blockage effects in arterial constriction and stenoses. Amrouche et al. [3] give experimental effects of pressure distribution due to blockage condition for grid turbulent flows for prisms for different small blockage ratios. Saltzman and Ayres [4] review various correlations of wind tunnel data to flight drag correlations for unswept, swept and delta wings, boattail effects, supercritical wings, sting support and Reynolds effects. Lombardi [5] experimentally gives effects of blockages on forces and moments for AGARD calibration models of different sizes for subsonic and transonic cases. Duraisamy et al. [6] has studied the wall interference effect on subsonic unsteady airfoil flows using a Navier-Stokes solver for the flow field over the airfoil and comparison with experimental results are also reported. It is seen that most of the studies are limited to low speed only and not much information of blockage and tunnel wall interference effect on pressure distribution on the body is reported especially in supersonic speeds.

In our previous effort, we considered the wind-tunnel wall to be truncated at some small distance further down from the nose of the model. This led to some difficulties for the Mach 1.6 case in comparison with shock reflections eluding appearance in the forward portion of the nose cone section. Also some spurious shock reflections form the leading edge of the wind tunnel wall were seen for Mach 1.6 and 3.0 cases. This could affect the estimates of the wall distances for the body to be clear of wall interference effects which was found to be adding to some extra predicted wind-tunnel wall distance. Hence the flow field was recomputed using a new domain where wind tunnel length is considered as starting from before the nose of tested model. To this effect there needs to be new domain to be defined made up of two parts which may be considered as containing a cut where this also models the transonic case for Mach 1.5 considered transonic, because of shape of body. As known from wind-tunnel testing of transonic bodies some porous slots are there in the wall. Here in this study we find that the domain so chosen give results which match with experimental

results of coefficient of pressure C_P and also the wall distances are found to be of better estimate.

In the present study the wall tunnel blockage and interference effect is studied on a launch vehicle heat shield portion using a computational fluid dynamics code UNS2D in supersonic flow conditions. The effect of blockage on the pressure distribution on the body is obtained and the wall interference is brought out clearly in Mach number and pressure pallets for different blockage ratios.

The Navier-Stokes solver UNS2D available in the Aerodynamics Research and Development Division (ARD), VSSC is a widely used CFD code and has shown to work well for several cases for aerodynamic flows associated with launch vehicles. The code solves the compressible Reynolds averaged Navier-Stokes equation using a Finite Volume Method and uses some of the state-of-the-art techniques like up-winding and implicit time integration for getting good quality results in a reasonable amount of computer time.

.

Formulation

The basic equations governing the fluid flows are the Reynolds averaged Navier-Stokes equations and are soved using a finite volume method . In conservation form, the axisymmetric N-S equation in differential form can be written

$$\frac{\partial U}{\partial t}+\frac{\partial F(U)}{\partial x}+\frac{\partial G(U)}{\partial r}+H=0$$

The vector of conserved variables U is r [ρ ρu ρv e]^T and the flux vectors F(U), G(U) and H(U) given by

$$F(U)=r\begin{bmatrix}\rho u\\ \rho u^2+p-\tau_{xx}\\ \rho uv-\tau_{xr}\\ u(p+e-\tau_{xx})-\tau_{xr}v+q_x\end{bmatrix}$$

$$G(U)=r\begin{bmatrix}\rho v\\ \rho uv-\tau_{xr}\\ \rho v^2+p-\tau_{rr}\\ v(p+e-\tau_{rr})-\tau_{xr}u+q_r\end{bmatrix}$$

$$H(U)=\begin{bmatrix}0\\ 0\\ -p+\tau_{\theta\theta}\\ 0\end{bmatrix}$$

The viscous shear terms are given by

$$\tau_{xx}=\frac{2}{3}\mu\left[2\frac{\partial u}{\partial x}-\left(\frac{\partial v}{\partial r}+\frac{v}{r}\right)\right]$$

$$\tau_{rr}=\frac{2}{3}\mu\left[2\frac{\partial v}{\partial r}-\left(\frac{\partial u}{\partial x}+\frac{v}{r}\right)\right]$$

$$\tau_{xr}=\mu\left[\frac{\partial v}{\partial x}+\frac{\partial u}{\partial r}\right]$$

$$\tau_{\theta\theta}=\frac{2}{3}\mu\left[2\frac{v}{r}-\left(\frac{\partial u}{\partial x}+\frac{\partial v}{\partial r}\right)\right]$$

The heat flux terms are given by

$$q_x=-k\frac{\partial T}{\partial x}$$

$$q_r=-k\frac{\partial T}{\partial r}$$

In the above equations, ρ is the density, u and v are the velocity components in the axial and radial directions, p is the pressure, e is the total energy, T is the temperature, μ is viscosity coefficient and k is the thermal conductivity. For easiness in computations, the above equations are non-dimensionalised. This is done by scaling all lengths by a reference length L, all velocities by free stream sonic velocity c_∞, viscosity by μ_∞, density by ρ_∞, pressure and total energy by $\rho_\infty c_\infty^{\,2}$, and temperature by T_∞ . The pressure p is calculated from the equation

$$P=(\gamma-1)\left(e-\rho(v^2+u^2)/2\right)$$

where γ is the ratio of specific heats. Perfect gas assumptions are assumed with the gas following the equation of state. The viscosity is assumed to vary with the temperature and the non-dimensional viscosity of the fluid is determined from the Sutherland formula given by

$$\mu=\frac{(1+S)T^{3/2}}{(T+S)}$$

with the constant $S=110.4/T_\infty$. The thermal conductivity is also assumed to vary in a similar fashion and can be computed from the Prandtl number.

Finite Volume Discretization

In the finite Volume method, the computational domain is subdivided into a network of meshes of finite volume and the governing fluid dynamics equations are used in the integral form. The Unknown vector U is required at the centroids of finite volume while the fluxes are calculated at the cell faces. In general co-ordinates, the flow equations in the integral form is given by

$$\frac{\partial}{\partial t}\int_V U\,dV + \int_S \vec{F}(U).d\vec{S} + \int_V H\,dV$$

Where V is the computational cell volume and S is the cell face area. Integration of the above governing equation on a computational cell (i,j), as shown in figure 1, and with the cell interfaces denoted by i±1/2 and j±1/2 gives

$$V\frac{\partial U}{\partial t} = -\left[S_{i+\frac{1}{2},j}\hat{F}_{i+\frac{1}{2},j} - S_{i-\frac{1}{2},j}\hat{F}_{i-\frac{1}{2},j} + S_{i,j+\frac{1}{2}}\hat{F}_{i,j+\frac{1}{2}} - S_{i,j-\frac{1}{2}}\hat{F}_{i,j-\frac{1}{2}}\right] - VH$$

Where,

$$\hat{F} = n_x F + n_y G$$

A Monotonic Upstream-Centered Scheme for Conservation Laws (MUSCL) -type approach is employed for the evaluation of the fluxes at the cell interfaces. The Van Albada limiter is used to avoid spurious oscillations of the solution. For calculations of split convective fluxes, the values of the primary variables at the cell face are needed. The left cell face values U^l obtained by forward extrapolation and the right cell face values U^r by backward extrapolation. Then the primary variables at the cell interfaces in the i^{th} direction is,

$$U^l{}_{i+\frac{1}{2},j} = U_{i,j} + (\varphi/4)\left[\kappa_1(U_{i+1,j} - U_{i,j}) + \kappa_2(U_{i,j} - U_{i-1,j})\right]$$

$$U^r{}_{i+\frac{1}{2},j} = U_{i+1,j} - (\varphi/4)\left[\kappa_1(U_{i+1,j} - U_{i,j}) + \kappa_2(U_{i+2,j} - U_{i+1,j})\right]$$

Values of $U^{l,r}$ in j direction are obtainable in the similar fashion. Several types of discretization can be obtained by using different values of κ_1 and κ_2 so as to control the degree of up-winding. In the above equations φ(R) is the limiter employed which is needed in flows involving shocks and is given by [7]

$$\varphi(R) = \frac{R^2 + R}{R^2 + 1}$$

$$R_{ij} = \frac{U_{i+1,j} - U_{i,j}}{U_{i,j} - U_{i+1,j}}$$

The inviscid convective part of fluxes at the cell interface is calculated using the Van Leer's flux vector splitting and is given by

$$F_{i+\frac{1}{2},j} = \left[F^+\left(U^l{}_{i+\frac{1}{2},j}\right) + F^-\left(U^r{}_{i-\frac{1}{2},j}\right)\right]$$

The viscous diffusive part of the fluxes is computed using central differencing. The time marching is done by an implicit time integration procedure with approximate factored bidiagonal scheme. The implicit time integration involves using of the approximated factorization and splitting of the fluxes. By using these methods block tri-diagonal equations are obtained which again can be simplified to get block bi-diagonal equations. The resulting implicit stage consists of a backward and forward sweep in every coordinate directions.

In order to capture the turbulent nature of the flow, the algebraic turbulence model of Baldwin-Lomax [8] is used to compute the Reynolds stresses. This is a two-layer model consisting of an inner law near the wall region and an outer law for regions away from wall. This model computes the turbulent viscosity to which the fluid viscosity is added to get the effective viscosity for computation. The basic assumption in this model is that the turbulent viscosity coefficient depends only on the instantaneous local flow variables. In spite of the simplicity, this zero equation model often gives good results compared to the more complex models like the two-equation k-ε models as reported by the study of Serpico et al [9]. The solver has already been applied for many complex problems like flow in the wing-elevon gap of Reusable Launch Vehicle [10], flow in the test section of a hypersonic nozzles [11] and base flow analysis of a single engine launch vehicle [12].

Boundary Conditions

Proper boundary conditions are to be used for getting the correct realistic solutions. In fact boundary conditions are the critical features driving the solution to the appropriate physical values. The following boundary conditions are used in this problem.

- At solid surface: no-slip boundary condition is employed which means that the velocity on the wall is stationary for a non-moving solid surface. An isothermal wall condition is used specifying the wall temperature as an input.
- At the downstream boundary: The flow variables are interpolated from inside cells if the flow is supersonic. If the flow is subsonic pressure boundary condition is used.
- At the inlet the free stream conditions are imposed.
- At the centre line, the symmetry boundary condition is employed.

Grid Generation

Grid generation is one of the most important and first step in the Computational Fluid Dynamics. This involves mainly discretising the computational domain into a number of meshes or cells in an orderly fashion. Although it looks to be a trivial task for simple bodies, it is really a challenging task when a complex configuration is to be discretised.

One of the simplest methods to generate grids over relatively simple body configurations is the algebraic grid generation technique. The grid can be clustered near any region of interest by using suitable stretching parameters. The clustering of grids is necessary near the solid wall so as to capture the boundary layer properly. Also in regions where high flow gradients due to expansion and shock the grids need to be clustered so as to capture the flow fields sharply. For the prediction of heat flux and shear stresses the first cell height from the solid walls will have to be in mi-

crons. The clustering of grids near the solid body are generated using the following formula

$$h = \frac{s(r - 1.0)}{(r^n - 1.0)}$$

where h is the first cell height, s is the distance, r is the stretching parameter and n is the number of divisions in that distance. The steps involved in the grid generation are:

- Defining the geometry and the coordinate system
- Defining the outer boundary which should be sufficiently away from body and there should not be much change in the flow field
- Choosing the regions of fine or coarse meshing. This includes regions near the solid walls where there will be strong gradients in velocities and temperatures because of boundary layer formation. The fine meshing is also needed in the regions where there is change in geometry.
- The selection of suitable stretching parameter to get the required clustering. As mentioned above a geometrical progression can be used for stretching the grids and the values can be adjusted for getting the required cell heights.

Figure 2 shows the schematic view of the body in test section. The figure shows the body configuration and the wind tunnel wall where solid wall boundary conditions are used. The centre line is also shown in the same figure. The geometrical body shown is the heat shield portion of a typical launch vehicle configuration. It consists of a spherical cap followed by a conical portion which is followed by a cylindrical part. The cylinder part is followed by a boat tail region with a specific angle after which a long cylinder is there. In launch vehicles the length of the body is very large compared to the diameter of the long cylinder portion considered. In this study the length to diameter is about 10. The distance from body to the tunnel wall is varied for getting different blockage ratios. A number of different blockage ratios are considered for simulations.

Figure 3a and 3b show the computational grid for two different blockage ratios considered. About 360 points are considered on the body geometry and 160 points are considered in the radial direction from the body to the tunnel wall. Suitable stretching parameters are used in the radial direction so that the grids are highly clustered both near the body and near the tunnel wall so as to capture the boundary layer near the solid wall. Clustering is also provided in the axial direction near various junctions where there are geometrical changes such as near the sphere-cone junction, cone-cylinder junction and also near the boat tail region.

Results and discussions

As mentioned earlier, the present study involves the numerical simulation of wall tunnel interference effect on a launch vehicle heat shield portion using computational fluid dynamics in supersonic flow conditions. The tunnel wall also is assumed to be circular in cross-section similar to the heat shield body.

Axi-symmetric simulations have been done for two supersonic Mach numbers of 1.5 and 3.0 for which wind tunnel experimental measurements are available. The Reynolds numbers corresponding to these Mach numbers are 3.0 and 1.5 million respectively. Free stream conditions are imposed as the initial conditions and the solutions are iterated to attain the converged steady state values by applying the proper boundary conditions mentioned above. The number of grids chosen along the body and in the radial directions is adequate to capture the flow parameters and no grid independence study is made here. Again sufficient numbers of iterations are made to ensure the convergence of the solutions shown. It is worth noting that one may encounter convergence problems for both the cases of Mach numbers for the mid range of blockage ratios considered which was overcome by reducing the CFL number to 0.1 and gradually increasing it up to 0.4 and this would require about 80000 to 1,20000 iterations for various cases of blockage ratios. Otherwise, the commonly required number of iterations is about 50000 to 60000.

As shown in figure 2, the ratio of the launch vehicle length to maximum diameter is about 10.0. A number of simulations have been done for different values of the ratios of the maximum diameter of the body ‘d’ to the tunnel wall diameter ‘D’. The different cases studied are for D/d values of 3.0, 4.0, 5.0, 6.5, 9.0, 11.5 and 14.0.

As a first step, the code is validated for free stream Mach numbers 1.5 and 3.0 flow conditions on the heat shield portion of a launch vehicle configuration for the surface pressure distribution along the axial length of the body. The numerical results are compared with the wind tunnel experimental data [13]. In figures 4a and 4b, the surface pressure distribution obtained from numerical simulations is plotted along with the measurement values. It can be seen that the comparison is very good in both the cases with the solver capturing all the flow features such as the expansions and compressions at different regions of the body. A slight distance downstream of the boat tail region on the long cylinder, the pressure will attain the free stream value and a zero pressure coefficient values will be obtained. This is clearly visible in both the figures where after x/d=2.5 the pressure coefficient value reaches zero and continues downstream till the end of the body.

Figure 5a and 5b show the convergence study carried out for D/d = 6.5 for Mach 1.5 flow and D/d = 4.0 for Mach 3.0 flow respectively. In each figures results from three different iterations, as mentioned in the figures where N is after a number of iterations, are shown. It can be seen that in both the cases all the three curves are indistinguishable from each other showing the convergence of the solution.

In figure 6a and 6b the surface pressure distribution is compared for blockage ratios of D/d=3.0 and 4.0 with the largest blockage ratio dimension of D/d=14.0 for both the Mach number 1.5 and 3.0. It can be seen that for lower blockage ratios of 3 and 4, oscillations are seen in pressure distributions which are due to the multiple shock reflection phenomena mentioned above. The sudden rise in the pressure is the location where the shocks from the tunnel wall hitting the body geometry. It can also be seen that the wall interference effect extends to the full length of the body. For the case D/d=14.5 the pressure distribution is smooth and as expected which show that there is no wall interference effect for this case. It is also seen that the effect is more for Mach1.5 case than Mach3.0 case.

In figure 7a and 7b the surface pressure distribution is shown for D/d=5.0 and 6.5 and compared with the largest blockage ratio case of D/d=14 for both the Mach numbers. Here it can be seen that for the Mach1.5 flow case the blockage effect is very much visible till the end of the body compared to the Mach3.0 flow case where the interference effect is very small. In fact for D/d=6.5 there is no interference effect for the Mach3.0 case and for D/d=5.0 the effect is visible at the end of the body only. It can be inferred that for D/d=5.0 with a vehicle length of x/d=8 the wall interference effect can be avoided for the Mach3.0 flow case which means that with a model of length x/d=8 the experiments can provide realistic measurement values.

In figure 8a and 8b the pressure distribution on the body is shown for D/d=9.0 and 11.5 and is compared with the case of D/d=14.0 for both the Mach numbers 1.5 and 3.0. From these figures it can be seen that the Mach3.0 flow case is completely interference free at these blockage ratio values. In the case of Mach1.5 flow case, the effect is limited beyond x/d=6.0 for D/d value of 9.0 and the effect is limited beyond x/d=8.5 for the D/d value of 11.5. Below these x/d values interference effect is not there and if the experimental model body length is below these values the results can be interference free and realistic also.

Figure 9 show the Mach number and pressure palettes for the case of free stream Mach number 1.5 for different blockage ratios as shown. The figure in the left side shows the Mach number palette and right side show the pressure palette. These figures clearly show the multiple shock phenomena features seen earlier in the surfacel pressure distributions. It can be seen that with the blockage ratio of D/d=3.0, the front detached shock itself could not be formed in the case of Mach 1.5 flow case in a proper way. For higher blockage ratios where the model diameter size is considerable relative to the tunnel wall distance, the detached shock in front of the body extends up to the tunnel wall and reflects back and this reflected shock on hitting the body is reflected back to the tunnel wall again in a weak way and a series of shock waves are seen which becomes weak downstream. As the blockage ratio decreases the detached shock in front of the body hits the tunnel wall at a slightly downstream distance and the reflected shock also hits the body at a little distance downstream.

In figure 10 the Mach number and pressure Palette of the case of Mach 3 free stream is shown for the blockage ratios as mentioned which also similar flow features as that for the Mach 1.5 case. It can be seen that the detached shock angle is lower compared to the case of Mach 1.5 case as expected. The shock emanating from the front of the body hits the tunnel wall at a little distance downstream compared to the Mach 1.5 case because of the lower angle of the shock. The reflected shock from the tunnel then hits the body again at a distance downstream. Because of this for the Mach 3.0 case a higher blockage ratio or smaller D/d value can be used for interference free testing.

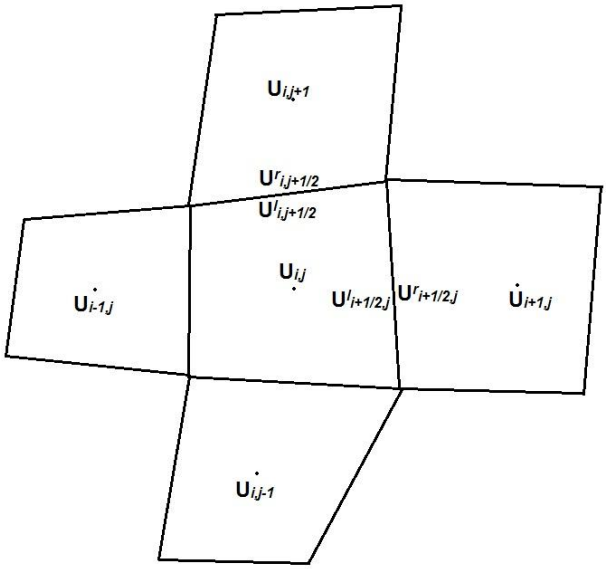

Fig. 1 Computational grid location variable

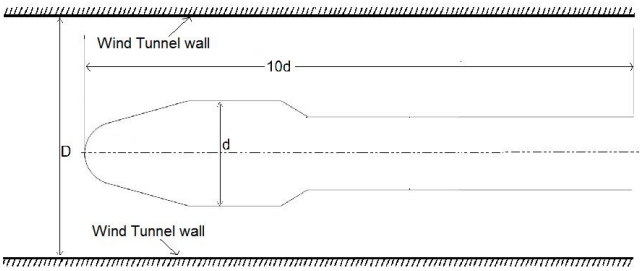

Figure 2 : Schematic diagram of body in test section of wind tunnel

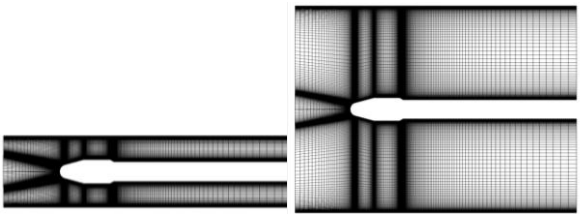

Fig. 3a Computational Grid for Case D/d =3.0 & Fig. 3b Computational Grid for Case D/d=9.0

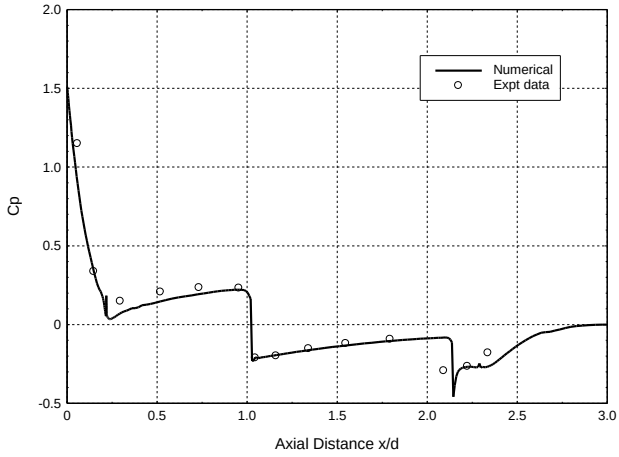

Fig 4a Surface Pressure Distribution M=1.5

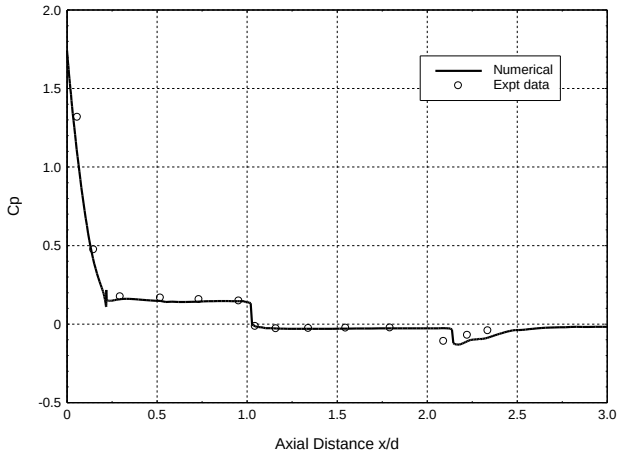

Fig 4b Surface Pressure Distribution M=3.0

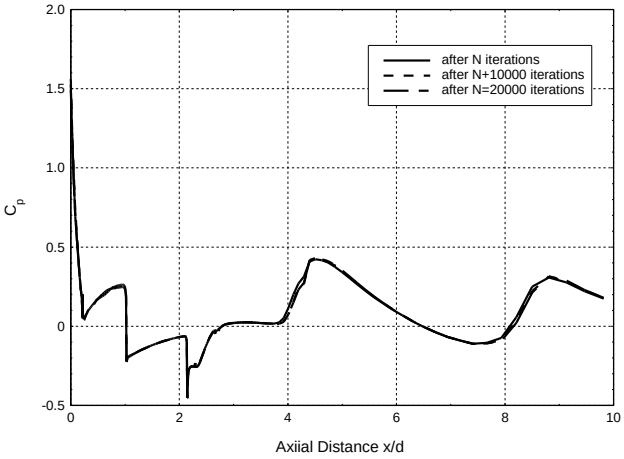

Fig 5a Convergence of Surface Pressure Distribution M=1.5

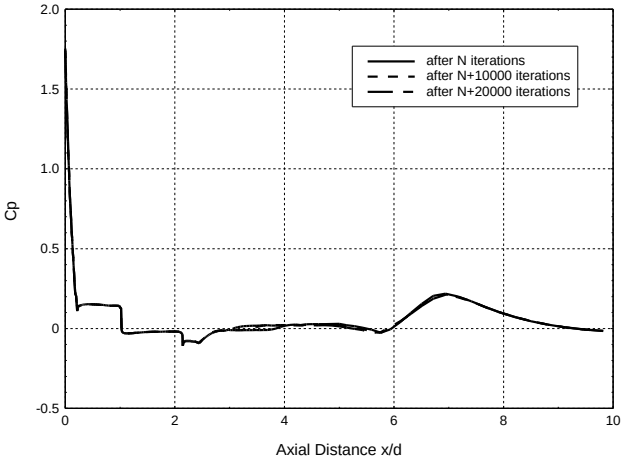

Fig 5b Convergence of Surface Pressure Distribution M=3.0

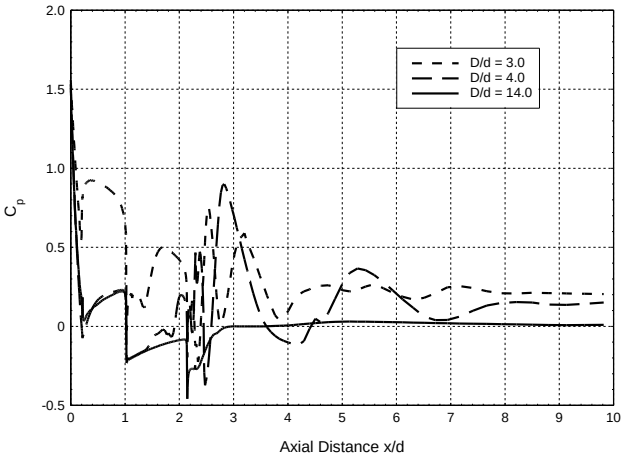

Fig 6a Pressure distribution for D/d 3.0,4.0 and 14.0 at M=1.5

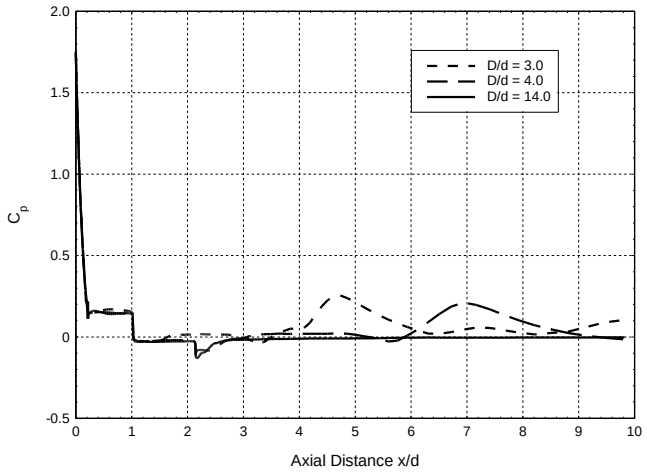

Fig 6b Pressure distribution for D/d 3.0,4.0 and 14.0 at M=3.0

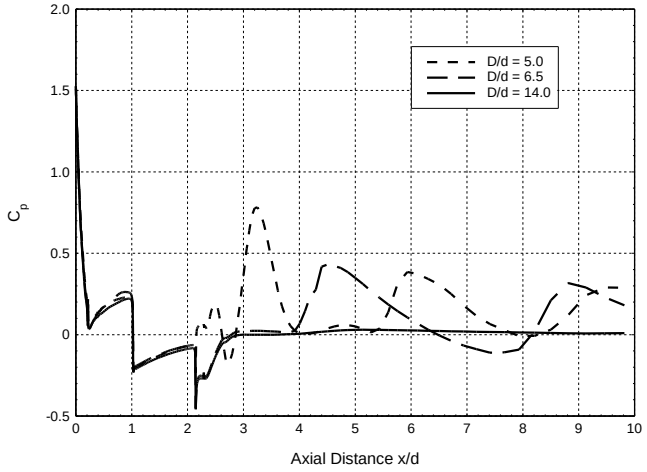

Fig 7a Pressure distribution for D/d 5.0,6.5 and 14.0 at M=1.5

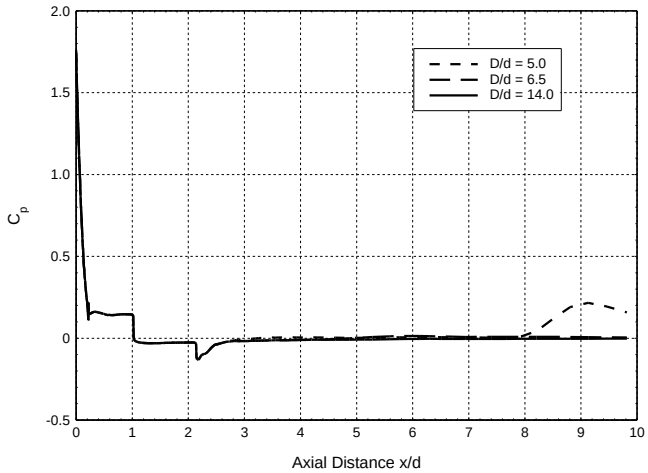

Fig 7b Pressure distribution for D/d 5.0,6.5 and 14.0 at M=3.0

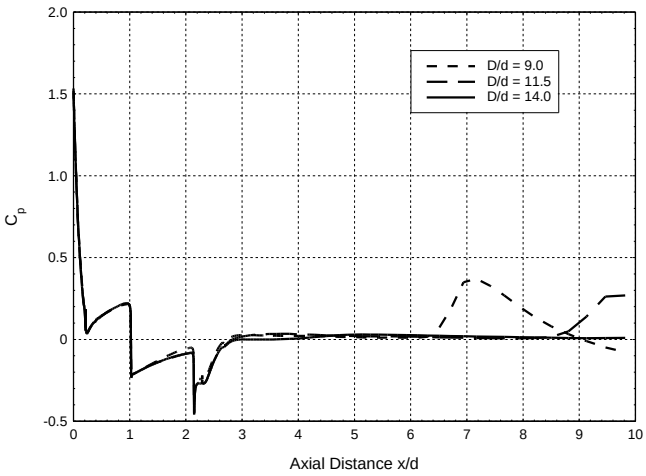

Fig 8a Pressure distribution for D/d 9.0,11.5 and 14.0 at M=1.5

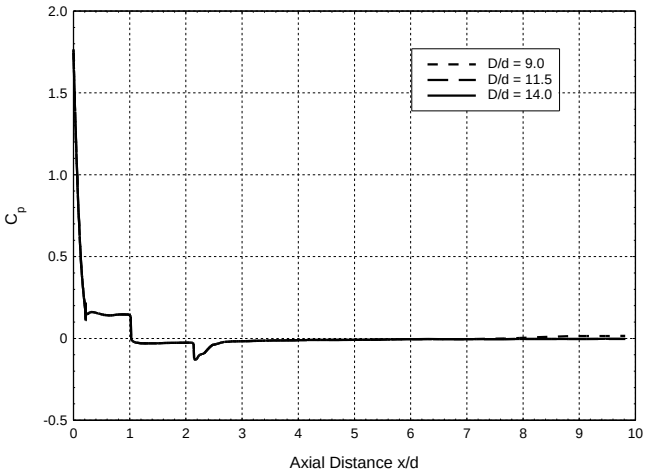

Fig 8b Pressure distribution for D/d 9.0,11.5 and 14.0 at M=3.0

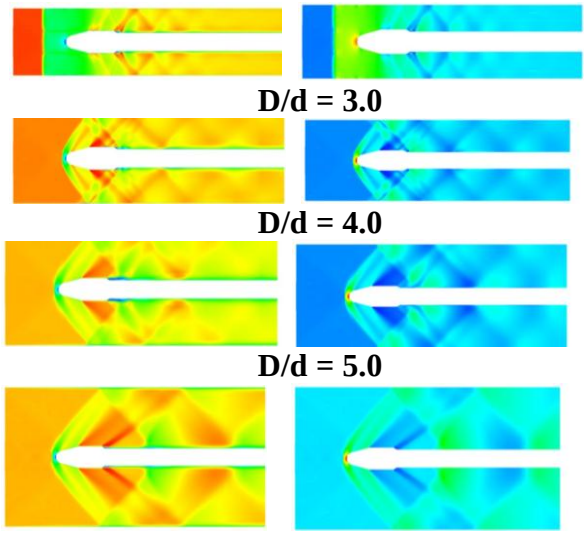

D/d = 6.5

Fig. 9a Mach number and pressure at M_∞ =1.5 for blockages ratios of 3.0 to 6.5

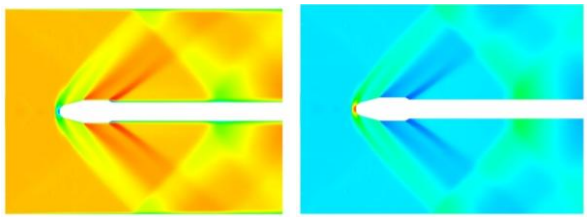

D/d = 9.0

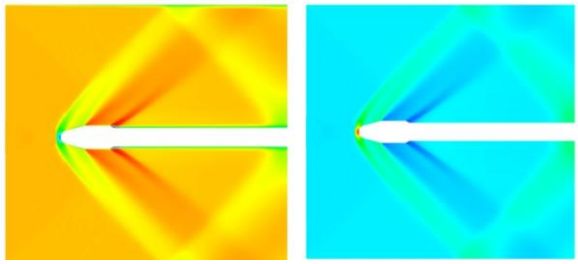

D/d = 11.5

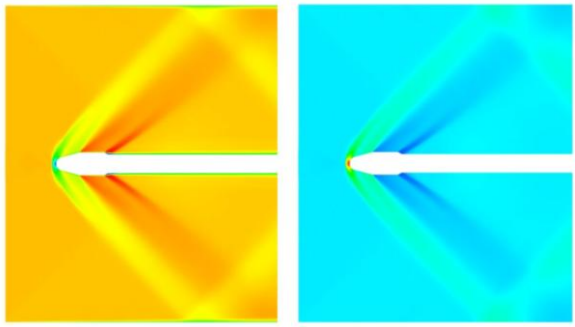

D/d= 14.0

Fig. 9b Mach number and pressure at M_∞ =1.5 for blockages ratios of 9.0 to 14.0

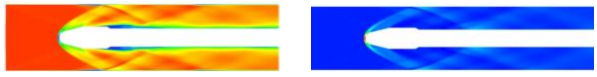

D/d = 3.0

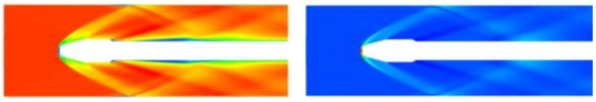

D/d = 4.0

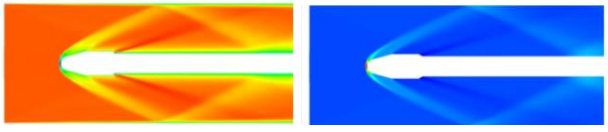

D/d = 5.0

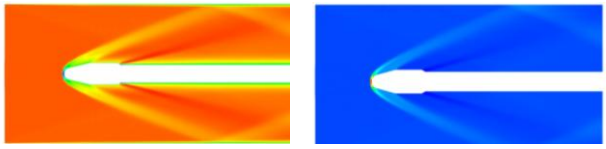

D/d= 6.5

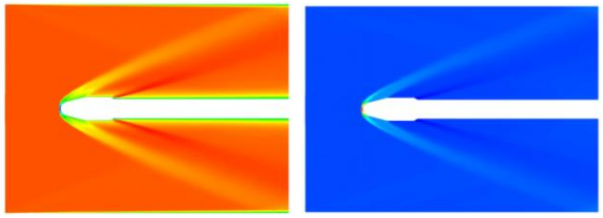

D/d= 9.0

Fig. 10 Mach number and pressure at M_∞ =3.0 for blockages ratios of 3.0 to 9.0

Conclusions

The numerical simulation of wall blockage and tunnel wall interference effect is studied on a payload fairing portion of a launch vehicle configuration. Computations have been done for two supersonic free stream Mach numbers of 1.5 and 3.0 for a number of blockage ratios and the pressure distribution on the body surface is obtained. The well known multiple shock phenomena associated with this type of problems are clearly captured by the solver and are clearly shown in the pressure distribution on the body where the pressure distribution show a series of oscillations because of the shock reflections from the tunnel wall. It is seen that with a higher blockage ratio the interference effect can be avoided by using a model of lower length. It is also seen that for Mach 3.0 flow case a higher blockage ratio value can be used without any interference effect than for the case of Mach 1.5 flow condition. The results are also presented in Mach number and pressure palette form which can give a better understanding of the physics of the problem and qualitatively as well as qualitatively show the flow features in this type of problems.

References

[1] Maciejewski M Osmolszi W and Poznanska P : Numerical simulation of blockage effects in wind tunnels, Proc 14th European Simulation Symposium, Verbraeck A and Krug W eds. SCS Europe BVBA 2002.

[2] Griffith M D, Houringan K and Thompson MC : Numerically modeling blockage on flow between flat plates, 15th Austrilian Fluid Mech Conf, U. Sidney, 13-17 Dec., 2004.

[3] Amrouche N, Dizene R and Laneville A : Observation of wind tunnel blockage effects on pressure distribution around rectangular prism in smooth and grid turbulent flows, Revue des Energies, Renouveleble SMEE'10 Bou Ismail Tipaza, pp21-26, 2010 1993.

[4] Saltzman E J and Ayers T G : A review of flight to wind tunnel drag correlations, AIAA Paper No 81-2475.

[5] Lombardi G and Morelli M : Analysis of some interfrence effects in a transonic wind tunnel, J Aircraft, Vol 32, No 3 1995..

[6] Duraisamy K, McCroskey W J Baeder : Analysis of wind tunnel wall interference effects on subsonic, unsteady airfoil flows, J Aircraft, Vol 44 No 5 2007.

[7] Van Albada GD, Van Leer B, Roberts WW Jr. : A comparative study of computational methods in cosmic gas dynamics, Astronomy & Astrophy., Vol 108, No 76, 1982.

[8] Bladwin, B. And Lomax, H., "Thin Layer Approximation for Algebraic Model for Separated Turbulent Flows", AIAA Paper 78-257, AIAA 16th Aerospace Science Meetings, 1978.

[9] Serpico, M., Schettino,A., Ciucci,A., Falconi,D. and Fabrizi,M., "Base Flow Predictions for a Lightsat Launcher at Supersonic Speeds", Journal of Spacecrafts and Rockets, V36, n2, 1999, pp. 247-254.

[10] Thomas, T. and Unnikrishnan, C., "CFD Studies for `the Wing-Elevon Gap region of a Hyprsonic Re-Usable Vehicle", 11th Annual CFD Symposium, Bangalore, India, Aug 11-12, 2009.

[11] Udaybhaskar, N., Kalimuthu, R. and Unnikrishnan, C., "Flow Field Analysis of Hypersonic Wind Tunnel Test Section with Mach6 Nozzle," National Conference on Wind Tunnel Testing (NCWT-03), Thiruvananthapuram, India, 23-24 August 2013.

[12] Tina, T. and Unnikrishnan, C., "Base Flow Studies for a Single-Engine Launch Vehicle Configuration," *Journal of Spacecraft and Rockets*, Vol. 48, No. 3, 2011, pp. 414-419..

[13] Kiselev, L.N., "The study of Distibution of Pressure Coefficients over the surface of Heat shield and Cryo stage (Model MkT51) in TsAGI Wind Tunnel T-114, Technical Report No.1151-93-96, 1993.